A non-symmetric integral approximation of large sliding frictional contact problems of deformable bodies based on ray-tracing

Poulios Konstantinos, Yves Renard

A non-symmetric integral approximation of large sliding frictional contact problems of deformable bodies based on ray-tracing

Konstantinos Poulios [*]   Yves Renard [†]

January 28, 2014

Abstract

In this paper a new approximation of frictional contact problems in finite deformation and large sliding is presented. The proposed method is based on an integral formulation and uses ray-tracing instead of a classical projection for defining a gap function. Compared to equivalent projection based formulations, the proposed method is more robust by being less sensitive to discretization discontinuities and permits a more efficient implementation. Appropriate mathematical treatment yields a tangent system which is simpler than in equivalent projection based formulations. The robustness and locking-free characteristics of the method are illustrated on some classical benchmark tests.

Keywords: frictional contact, finite elasticity, large sliding contact, finite element method.

1 Introduction

Frictional contact between deformable solids undergoing large deformations is still considered as a difficult problem to solve numerically. This is because it involves geometrical and mechanical quantities that depend on an a priori unknown mapping between the surfaces in contact. Many efforts for providing robust and efficient numerical solutions to this problem have been made, including: 1) the classical node-to-segment method in combination with smoothing techniques, 2) mortar and Nitsche methods as well as 3) contact segment and contact domain methods.

The first two categories represent asymmetric formulations, in the sense that the contacting surfaces are treated differently by distinguishing between a master (or mortar or target) and a slave (or non-mortar or contactor) surface. On the contrary, the methods of the third category (see for instance [3, 10, 16]) are by their nature symmetric and they are consequently directly applicable to cases like simultaneous contact between three or more solids as well as self-contact, where non-symmetric formulations would require special treatment. However, contact segments definition and contact domain triangulation are not guaranteed for any arbitrary three dimensional geometry, limiting the adoption of this category of contact discretizations.

The asymmetry introduced by the first two categories of contact formulations into the treatment of the contacting surfaces, is because of quantities that have to be defined on only one of the contacting surfaces. These quantities are:

---

[*]Department of Mechanical Engineering, Technical University of Denmark, Nils Koppels Allé, Building 404, 2800 Kgs. Lyngby, Denmark. email: `kopo@mek.dtu.dk`

[†]Université de Lyon, CNRS, INSA-Lyon, ICJ UMR5208, LaMCoS UMR5259, F-69621, Villeurbanne, France. email: `yves.renard@insa-lyon.fr`

1

1.a) Lagrange multipliers (applies to node-to-segment and mortar methods) and/or contact nodes (applies to the node-to-segment method).

1.b) Quadrature points for numerical integration of contact terms (applies to mortar and Nitsche methods).

2) The contact normal direction.

Theoretically it is possible to define each of these quantities on one of the contacting surfaces arbitrarily. However, when a contact approximation involves both Lagrange multipliers and numerical integration (see mortar method), no advantage can be seen in defining the Lagrange multipliers and the quadrature points on different surfaces. For this reason, it is assumed that these two quantities will always be defined on the same surface which is typically referred as the slave surface. The slave surface is also the side featuring the contact nodes in the case of the node-to-segment method.

Traditionally, the contact normal direction is defined on the master surface. This convention originates from the classical node-to-segment method, where for non-smooth meshes, defining a normal direction on the contact nodes is ambiguous. Although this restriction is not present in mortar or Nitsche contact formulations, these methods usually define the contact normal according to the master surface. Quadrature points are projected from the slave onto the master surface in a similar way like contact nodes are projected in the node-to-segment method. The convention of a contact normal perpendicular to the master surface is followed e.g. in the large deformation contact approximations presented in [1, 8, 15, 6].

The possibility of defining the contact normal on the slave surface is strongly under-represented in the computational contact mechanics literature. A justification for avoiding this possible option is also hard to find. In the present paper, based on the augmented Lagrangian non-symmetric formulation from Alart and Curnier [1], an integral approximation of large sliding frictional contact problems is derived, which utilizes the slave surface both for defining the contact normal and Lagrange multipliers along with a numerical integration scheme for the contact constraint terms. This choice results to a formulation which does not depend on the curvature of the master surface and to an optimality system which is not discontinuous across mesh vertices or edges, without the need for applying any smoothing technique.

An additional advantage of the presented method is that the mapping between points on the slave and the master surfaces is unambiguous and corresponds to a one-dimensional ray-tracing problem, irrespective if the contact problem space is two-dimensional or three-dimensional. On the contrary, the classical point to surface projection in a three-dimensional space is a two-dimensional problem.

The here proposed approximation is one of the few ones in the computational contact mechanics literature that define the contact normal, the Lagrange multipliers and the quadrature points on the same surface (slave). Other occurrences of this strategy are available in [18] in the segment-to-segment approach, in [11] in a somehow similar manner as part of a mortar contact approximation, in [15] as part of a Nitsche contact approximation in the small deformation framework, as well as in [2] for expressing multibody dynamic problems with contacts. In [17], ray-tracing is used in combination with classical projection in order to define contact segments in two-dimensional problems. The ray-tracing method is also used in [14] for contact detection and in the field of computer graphics, in [5] where a ray-tracing based collision detection method is formulated as an explicit penalized contact algorithm.

Another important characteristic of the proposed method is the integral approximation of the contact with friction condition. There is a very few occurrence of such a strategy in the computational contact mechanics literature. As far as we checked, only [7] and [13] refer to a

comparable strategy. The difference between a pointwise (node-wise or quadrature pointwise) and an integral approximation is detailed in [12]. Even in mortar and multiplier based methods, the contact and friction conditions are usually prescribed on the multiplier finite element nodes. The principle of the integral approximation is directly to incorporate an equivalent formulation of the frictional contact condition in term of an equation in the weak formulation. Doing so, the weak formulation itself is no-longer a weak inequality even in the continuous case. The main advantage of this approach is the fact that it is no longer necessary to prescribe some constraints on the multiplier (negativity of the contact pressure, friction bound on the tangential component) because it is already weakly included in the formulation. As an interesting consequence, the formulation is independent of the finite element methods chosen to describe the deformation and the multiplier.

2 Problem setting and notations

We denote by $\Omega \subset \mathbb{R}^d$ ($d = 2$ or 3) the reference configuration of one or several elastic bodies (Ω may have several connected components, as in Fig. 1) and the finite deformation

$$
\begin{array}{rcl}
\varphi : \Omega & \longrightarrow & \mathbb{R}^d \\
X & \longmapsto & x = \varphi(X),
\end{array}
$$

which is also often written in terms of $\varphi(X) = X + u(X)$ with $u(X)$ the displacement relatively to the reference configuration. The deformed configuration will be denoted $\Omega_t = \varphi(\Omega)$. We are interested in the finite deformation of the elastic body(ies) submitted to a contact constraint on a part of the boundary between a slave surface and a master one. This means that we consider a part of the boundary of Ω, we denote $\Gamma^S \subset \partial\Omega$ being a slave (or contactor) surface and another part $\Gamma^M \subset \partial\Omega$ being the master (or target) surface and we consider a non-penetration condition between the corresponding deformed surfaces $\Gamma_t^S = \varphi(\Gamma^S)$ and $\Gamma_t^M = \varphi(\Gamma^M)$ (see Fig. 1). In the description of the contact conditions, we will denote $X \in \Gamma^S$ a generic point of the slave surface in reference configuration, N_X the unit outward normal vector to Γ^S at X, $x = \varphi(X)$ the corresponding point of the deformed configuration, $n_x = ((\nabla\varphi(X))^{-T} N_X)/\|(\nabla\varphi(X))^{-T} N_X\|$ the unit outward normal vector to Γ_t^S at x ($\nabla\varphi(X)$ denotes the gradient of φ at point X which is a $d \times d$ matrix and $(\nabla\varphi(X))^{-T}$ the transposed inverse of this gradient). We will determine $y \in \Gamma_t^M$ the point of the deformed master surface in potential contact with x and $Y \in \Gamma^M$ the point of the reference master surface such that $y = \varphi(Y)$. The vectors N_Y and n_y represent the unit normal vector of the master surface in reference configuration at Y and in deformed configuration at y, respectively.
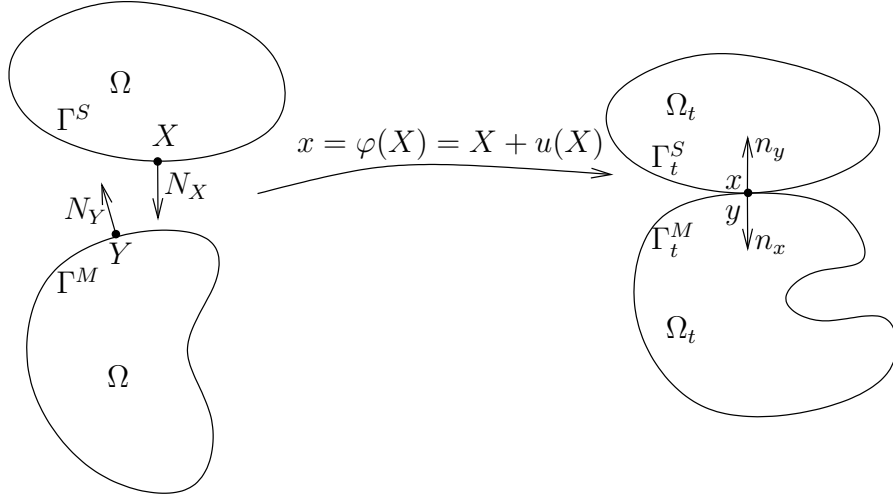
Figure 1: *Reference configuration Ω, deformed one Ω_t, deformation φ.*

In the following, the directional derivative of a quantity A, at the point ξ, with respect to a variable ξ in the direction $\delta\xi$ will be denoted by $\delta_\xi A(\xi)[\delta\xi]$. In other word

$$\delta_\xi A(\xi)[\delta\xi] = \lim_{\varepsilon \to 0} \frac{A(\xi + \varepsilon\delta\xi) - A(\xi)}{\varepsilon},$$

when this limit exists. When there is no possible ambiguity on the argument of the quantity A, we could write $\delta_\xi A[\delta\xi]$ instead of $\delta_\xi A(\xi)[\delta\xi]$.

We suppose that we consider the equilibrium or the quasi-static evolution of the body(ies). Since the choice of the constitutive law is not central in the description of our contact approximation, we will simply denote the global potential energy by

$$J(\varphi),$$

without going into details in the description of the different possible terms that may constitute this energy. As an example, if a simple equilibrium under a gravity force is considered, the potential energy can have the form

$$J(\varphi) = \int_\Omega W(\varphi(X))dX - \int_\Omega (-\rho\mathcal{G}e_z) \cdot \varphi(X)dX,$$

where W is the potential of an hyper-elastic constitutive law, ρ is the density in reference configuration, $\mathcal{G}$ the gravity constant and e_z the vertical direction. Of course some additional terms can be considered such as boundary loads.

Some Dirichlet conditions can also be considered. The standard way is to prescribe them both on the deformations and on the test function of the weak formulation. For the sake of simplicity of the presentation, we will not mention it in the following.

3   Ray-tracing instead of projection

The most used strategy to express a large sliding contact condition (see for instance [1, 8, 15]) is to define the gap between a slave (or contactor) surface and a master (or target) one in terms of

the distance between a point x of the slave surface and its projection y on the master one (see Fig. 2 (a)).

The ray-tracing strategy we use in this paper is slightly different in the sense that the gap will be defined as the distance between a point x of the slave surface and the point y corresponding to the closest intersection of the master surface with the line passing through the point x and having direction vector n_x (see Fig. 2 (b)).

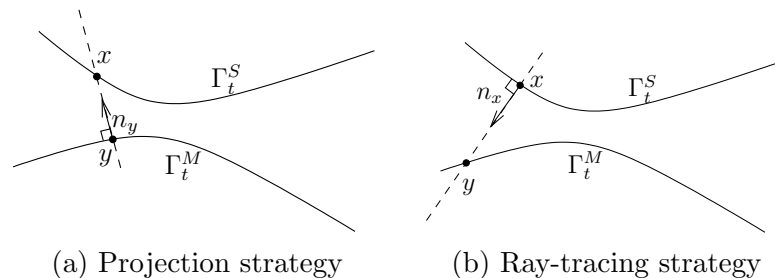(a) Projection strategy (b) Ray-tracing strategy

Figure 2: *Comparison between projection and ray-tracing strategies.*

The two strategies are in fact closely related since the orthogonality of n_x to the slave surface implies that in the ray-tracing strategy, the point x is the projection of y on the slave surface. Thus, it can be viewed as a reciprocal strategy with respect to the projection.

The main advantage of the ray-tracing strategy will appear in the construction of the weak formulation. It will mainly result on the fact that the unit normal vector n_x has a simpler derivative as n_y.

It can also be noted two additional advantages. The first one is that, from a computational viewpoint, ray-tracing is a one-dimensional search which allow faster algorithms to be computed than the projection. The second one is that the probability to come across a non regular point (corner of the body or simply element frontiers) is negligible for the ray-tracing strategy and very frequent for the projection (see Fig. 3, the projection is somehow attracted by convex non-regular points) causing some problems to define n_y.
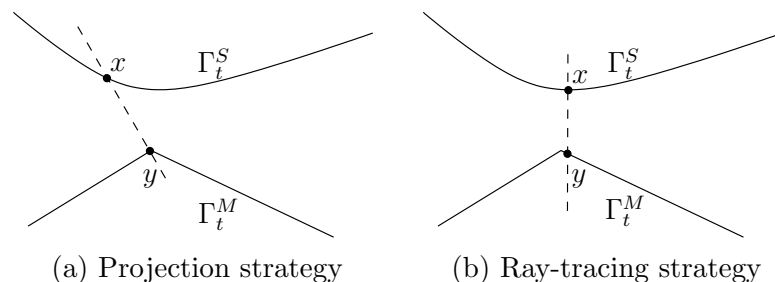

(a) Projection strategy (b) Ray-tracing strategy

Figure 3: *The projected point y falls on a convex non-regular point from a large set of slave points. On the contrary, with the ray-tracing strategy there is a negligible probability to fall on a non regular point.*

4 A weak formulation in the frictionless case

In this section, we build the weak formulation in the frictionless case. The formulation will be extended to friction in Section 5.

As introduced in the previous section, for each point $X \in \Gamma^S$ we associate $x = \varphi(x)$ on Γ_t^S and we denote y the nearest point (if it exists) of the master surface Γ_t^M which lies in the line passing through the point x and having direction vector n_x. We will denote by $\Gamma_c^S \subset \Gamma^S$ the part of the slave surface in reference configuration for which such an y exists.

For $X \in \Gamma_c^S$, we define the normal gap by

$$g(X) = n_x \cdot (y - x).$$

Then, the equilibrium of the elastic body submitted to a frictionless contact condition between the slave and the master surface can be represented by the saddle point of the following Lagrangian:

$$\mathscr{L}(\varphi, \lambda_N) = J(\varphi) + \int_{\Gamma_c^S} \lambda_N(X) g(X) d\Gamma, \tag{1}$$

under the constraint $\lambda_N \leq 0$, where $\lambda_N : \Gamma^S \to \mathbb{R}$ is the Lagrange multiplier corresponding to the constraint $g \geq 0$ which can be assimilated as a normal contact stress (in the reference configuration).

In order to determine the optimality system of this Lagrangian, we need the directional derivative of the normal gap with respect to the deformation. Still assuming sufficient regularity, a basic calculation leads to

$$\delta_\varphi g[\delta u] = -\frac{n_y}{n_x \cdot n_y} \cdot (\delta u(X) - \delta u(Y) + g(X) \delta_\varphi n_x[\delta u]), \tag{2}$$

where $\delta_\varphi n_x[\delta u]$ is the directional derivative of the unit normal vector n_x which is given by:

$$\delta_\varphi n_x[\delta u] = -(I - n_x \otimes n_x)(\nabla \varphi(X))^{-T} \nabla \delta u^T(X) n_x, \tag{3}$$

where I is the $d \times d$ identity matrix and $n_x \otimes n_x$ is the tensor product matrix of n_x by itself which could also be written $n_x n_x^T$. Note that $(I - n_x \otimes n_x)$ is simply the projection onto the tangent plane to the slave surface.

At this stage, one may remark that the directional derivative of the normal gap is slightly more complicated than the one obtained with the projection strategy (see the expression, for instance in [8, 15]). However, we will be able to simplify the expression.

As a consequence, the optimality system of the Lagrangian (1) can be expressed as follows:

$$\begin{cases} \delta_\varphi J[\delta u] - \int_{\Gamma_c^S} \lambda_N \frac{n_y}{n_x \cdot n_y} \cdot (\delta u(X) - \delta u(Y) + g(X) \delta_\varphi n_x[\delta u]) \, d\Gamma = 0 \quad \forall \delta u, \\ \int_{\Gamma_c^S} (\lambda_N - \delta \lambda_N) g d\Gamma \geq 0 \quad \forall \delta \lambda_N \leq 0. \end{cases}$$

Of course, we remark that the unit normal vector n_y to the master surface appears in this optimality system. This represents a real difficulty, since in order to obtain the tangent system (for instance to apply a Newton algorithm) one needs to obtain the derivative of the optimality system. However, the unit normal vector n_y is not even continuous (for instance on corners or on element frontiers). We will circumvent this difficulty remarking that either contact occurs on

a small surface and in this case $\dfrac{n_y}{n_x \cdot n_y} = n_x$ or contact does not occur and $\lambda_N = 0$. This means that we can always replace the expression $\dfrac{n_y}{n_x \cdot n_y}$ by n_x in the optimality system. Remarking additionally that $n_x \cdot \delta_\varphi n_x[\delta u] = 0$, this leads to the following simplified system:

$$
\begin{cases}
\delta_\varphi J(\varphi)[\delta u] - \displaystyle\int_{\Gamma_c^S} \lambda_N n_x \cdot (\delta u(X) - \delta u(Y))d\Gamma = 0 \quad \forall \delta u, \\[4mm]
\displaystyle\int_{\Gamma_c^S} (\lambda_N - \delta\lambda_N)g d\Gamma \geq 0 \quad \forall \delta\lambda_N \leq 0.
\end{cases}
\tag{4}
$$

The advantage of this system is that only the unit normal vector n_x intervenes and that the directional derivative of y with respect to φ is directly given by the fact that

$$y = x + gn_x,$$

so that

$$\delta_\varphi y[\delta u] = \delta u(X) + \delta_\varphi g[\delta u]n_x + g\delta_\varphi n_x[\delta u].\tag{5}$$

Thus, y is continuous with respect to φ and the directional derivative does not depend on the curvature of the master surface. This is a crucial advantage on the projection strategy for which the projected point is discontinuous in several situations and the directional derivative needs the computation of the curvature of the master surface (see [8, 15, 6]). As a conclusion, the simplified system (4) is continuous with respect to the deformation φ (its finite element discretization will be piecewise $\mathscr{C}^1$ regular). This property seems not to be possible to obtain with a projection strategy (without a smoothing strategy of the contact surfaces as proposed in [15])

Note that action-reaction Newton's law is obviously satisfied in (4) and that the price for simplicity of this system is a certain loss of symmetry.

We could directly make a finite element approximation of system (4) with for instance a nodal approximation of the contact condition. However, a nodal contact condition would lead to the use of the unit normal vector n_x at finite element nodes which are most of the time on the frontier between elements. In the latter case, except for conformal $\mathscr{C}^1$ finite elements, the unit normal vector is not well defined. This obliges to define a mean unit normal vector (see [11]). This is not a huge difficulty, however we prefer here to circumvent this difficulty by approximating the contact in an integral way. See [12] for a review on different approximations of the contact condition in a small deformation framework.

In order to obtain an integral formulation, we deduce our weak formulation from Alart-Curnier augmented Lagrangian (see [1]) adapted to our case:

$$
\mathscr{L}_r(\varphi, \lambda_N) = J(\varphi) + \int_{\Gamma_c^S} \lambda_N(X)g(X)d\Gamma - \frac{1}{2r}\int_{\Gamma_c^S}(\lambda_N + rg)_+^2 d\Gamma + \frac{r}{2}\int_{\Gamma_c^S}g^2 d\Gamma,
\tag{6}
$$

where $(\cdot)_+$ is the positive part $((x)_+ = x$ if $x \geq 0$, $(x)_+ = 0$ if $x < 0)$ and $r > 0$ is the augmentation parameter. Note that use of $\mathscr{L}_r$ does not represent an approximation or a penalization of the contact condition. The two Lagrangian $\mathscr{L}_r$ and $\mathscr{L}$ have the same saddle points (neglecting regularity issues). The optimality system of this augmented Lagrangian is the following:

$$
\begin{cases}
\delta_\varphi J(\varphi)[\delta u] - \displaystyle\int_{\Gamma_c^S}(\lambda_N + rg)_- \delta_\varphi g[\delta u]d\Gamma = 0 \quad \forall \delta u, \\[4mm]
-\dfrac{1}{r}\displaystyle\int_{\Gamma_c^S}(\lambda_N + (\lambda_N + rg)_-)\delta\lambda_N d\Gamma = 0 \quad \forall \delta\lambda_N,
\end{cases}
\tag{7}
$$

7

where $(\cdot)_-$ is the negative part $((x)_- = (-x)_+)$.

In order to simplify the system, we still replace $\dfrac{n_y}{n_x \cdot n_y}$ by n_x and we choose the most non-symmetric formulation (see [12]) by replacing in the first line of (7) the term $(\lambda_N + rg)_-$ by $-\lambda_N$. This leads to the following system:

$$\begin{cases} \delta_\varphi J(\varphi)[\delta u] - \displaystyle\int_{\Gamma_c^S} \lambda_N n_x \cdot (\delta u(X) - \delta u(Y)) d\Gamma = 0 \quad \forall \delta u, \\ -\dfrac{1}{r} \displaystyle\int_{\Gamma_c^S} (\lambda_N + (\lambda_N + rg)_-) \delta \lambda_N d\Gamma = 0 \quad \forall \delta \lambda_N. \end{cases} \tag{8}$$

We thus obtain a system which is both continuous with respect to the deformation and without constraints. It is non-symmetric, however, at least in the small deformation framework, the numerical tests in [12] show that symmetry is not necessarily an advantage for the convergence of Newton's algorithm (some non-symmetric formulations are performing better than symmetric ones).

5   Augmented Lagrangian strategy for the Coulomb friction case

Coulomb's law connects the sliding velocity to the tangential and normal stresses. This means that it normally applies to transient problems, even if some equilibrium solutions with Coulomb friction can make sense. To extend the problem to friction, we will consider a quasi-static process and still consider that $J(\varphi)$ represent the total potential energy. We denote by

$$V^r(X),$$

the relative velocity. In a quasi-static process, $V^r(X)$ can be written for instance

$$V^r = \frac{1}{\Delta t}(\varphi(X) - \varphi(Y) - \varphi_{n-1}(X) - \varphi_{n-1}(Y)),$$

where φ_{n-1} is the deformation at the previous time step.

Then, system (8) can be easily extended to Coulomb friction, using similar techniques as in [1, 12] and this gives the following system

$$\begin{cases} \delta_\varphi J(\varphi)[\delta u] - \displaystyle\int_{\Gamma_c^S} \lambda \cdot (\delta u(X) - \delta u(Y)) d\Gamma = 0 \quad \forall \delta u, \\ -\dfrac{1}{r} \displaystyle\int_{\Gamma_c^S} (\lambda - F(\lambda, g, V^r, n_x)) \cdot \delta \lambda d\Gamma = 0 \quad \forall \delta \lambda, \end{cases} \tag{9}$$

where $\lambda : \Gamma_c^S \to \mathbb{R}^d$ is now a vector field and F is the following map:

$$F(\lambda, g, V^r, n) = -(\lambda \cdot n + rg)_- n + P_{B_T(\mathscr{F}(\lambda \cdot n + rg)_-)}(\lambda - rV^r),$$

with $\mathscr{F}$ the friction coefficient and $P_{B_T(\tau)}$ the projection on the ball centered on 0 of radius τ on the tangent plane, i.e.

$$P_{B_T(\tau)}(v) = \left| \begin{array}{ll} (I - n_x \otimes n_x)v & \text{if } \|(I - n_x \otimes n_x)v\| \leq \tau, \\ \tau \dfrac{(I - n_x \otimes n_x)v}{\|(I - n_x \otimes n_x)v\|} & \text{otherwise.} \end{array} \right.$$

8

Note that in System (9), the Coulomb law is expressed on λ which is the contact force density in the reference configuration. The contact force density of the deformed configuration is

$$\frac{\lambda}{\|(\nabla\varphi(X))^{-T}N_X\|\det(\nabla\varphi(X))}$$

The fact that Coulomb's law is not sensitive to the magnitude of couple of tangential and normal contact forces allows to express it on the reference configuration. This would not be the same for some more elaborated laws, for instance when the friction threshold depends non-linearly of the contact pressure.

6 Finite element approximation and tangent system

Since System (9) is an unconstrained problem, a standard Galerkin procedure can be applied by choosing two finite element spaces for the deformation and the contact stress. In particular, it is not necessary to further specify in what sense the normal contact stress is non-positive or in what sense the Coulomb friction law is fulfilled since it is already taken into account.

Let $V^h \subset H^1(\Omega; \mathbb{R}^d)$ and $W^h \subset L^2(\Gamma^S; \mathbb{R}^d)$ be two finite element spaces. It is assumed that V^h takes into account any possible Dirichlet condition. Then, the finite element approximation of System (9) reads as

$$\begin{cases} \delta_\varphi J(\varphi^h)[\delta u^h] - \displaystyle\int_{\Gamma_c^S} \lambda^h \cdot (\delta u^h(X) - \delta u^h(Y))d\Gamma = 0 & \forall \delta u^h \in V^h, \\[3mm] -\dfrac{1}{r}\displaystyle\int_{\Gamma_c^S}(\lambda^h - F(\lambda^h, g, V^r, n_x)) \cdot \delta\lambda^h d\Gamma = 0 & \forall \delta\lambda^h \in W^h. \end{cases} \tag{10}$$

Note that System (10) is Lipschitz-continuous with respect to the pair φ^h, λ^h and piecewise $\mathscr{C}^1$ which a priori allows the use of a generalized Newton method to solve it. We give now the expression of the tangent system corresponding to (10), since it is necessary to the use of a generalized Newton algorithm. It consists in finding $\delta\mu^h \in W^h, \delta v^h \in V^h$ solution to

$$\begin{cases} \delta_{\varphi,\varphi}^2 J(\varphi^h)[\delta u^h, \delta v^h] - \displaystyle\int_{\Gamma_c^S} \delta\mu^h \cdot (\delta u^h(X) - \delta u^h(Y))d\Gamma \\[3mm] \quad + \displaystyle\int_{\Gamma_c^S} \lambda^h \cdot (\nabla\delta u^h(Y)(\nabla\varphi^h(Y))^{-1}(\delta_\varphi y[\delta v^h] - \delta v^h(Y))d\Gamma \\[3mm] \quad = -\delta_\varphi J(\varphi^h)[\delta u] + \displaystyle\int_{\Gamma_c^S} \lambda^h \cdot (\delta u^h(X) - \delta u^h(Y))d\Gamma \quad \forall \delta u^h \in V^h, \\[3mm] -\dfrac{1}{r}\displaystyle\int_{\Gamma_c^S}\Big[(I - \delta_\lambda F)\delta\mu^h - \delta_g F\delta_\varphi g[\delta v^h] - \delta_{V^r} F\delta_\varphi V^r[\delta v^h] - \delta_n F\delta_\varphi n_x[\delta v^h]\Big] \cdot \delta\lambda^h d\Gamma \\[3mm] \quad = \dfrac{1}{r}\displaystyle\int_{\Gamma_c^S}(\lambda^h - F) \cdot \delta\lambda^h d\Gamma \quad \forall \delta\lambda^h \in W^h, \end{cases} \tag{11}$$

where $\delta_{\varphi,\varphi}^2 J(\varphi^h)[\delta u^h, \delta v^h]$ is the second directional derivative of $J(\varphi^h)$, $\delta_\varphi g[\delta v^h]$ is given by (2), $\delta_\varphi n_x[\delta v^h]$ by (3), $\delta_\varphi y[\delta v^h]$ by (5), $\delta_\varphi V^r[\delta v^h]$ is to be determined knowing the expression of V^r and $\delta_\lambda F$, $\delta_g F$, $\delta_{V^r} F$ and $\delta_n F$ are the partial derivative of F. For completeness, the partial derivatives of the map F are given in Appendix A.

7   A few implementations details

An implementation of the presented approximation has been realized in the open-source finite element library Getfem++ [1]. A rather simple heuristic contact detection has been used for computing contact pairs between non-matching meshes efficiently and is described in the user documentation of Getfem++ [2]. In particular, R-tree based influence boxes are used to find the faces in front of a particular Gauss point in computational time of logarithmic complexity. For curved faces, a Newton algorithm is used to perform the ray-tracing. A release distance is applied to retain only contact pairs representing a contact which is likely to occur within the current load step.

On the part $\Gamma^S \setminus \Gamma_c^S$ of Γ^S which is far from contact (for which no corresponding point or too far away point has been found by the ray-tracing), the term

$$-\frac{1}{r} \int_{\Gamma^S \setminus \Gamma_c^S} \lambda^h \cdot \delta\lambda^h d\Gamma$$

is added to enforce the multiplier to be zero.

Despite the fact that the weak formulation leads to integrate low regular functions on the contact boundary, a few Gauss points per element edge/face was necessary to obtain an optimal accuracy (in the sense that an increase of the number of Gauss points did not lead to a better accuracy). Typically three Gauss points per edge in 2D and nine Gauss points per element face in 3D are sufficient, as the numerical examples in the next section demonstrate.

8   Numerical experiments

In this section we present numerical results for two two-dimensional problems that are typically used for testing large sliding contact algorithms and one three-dimensional problem including self-contact.

All three examples presented below are based on a neo-Hookean material law according to the following strain energy density function:

$$W(\varphi) = \frac{\mu}{2}\left(i_1 \cdot i_3^{-1/3} - 3\right) + \frac{\kappa}{2}\left(i_3^{1/2} - 1\right)^2,$$

with i_1 and i_3 respectively representing the first and the third invariants of the Cauchy-Green tensor defined as $\nabla\varphi(X)^T \nabla\varphi(X)$. The initial shear modulus μ and bulk modulus κ can be calculated from the corresponding Young's modulus and Poisson's ratio values provided in each numerical example.

8.1   Elastic ring on block

The first numerical example corresponds to the so called ring-on-block problem described in [15] and also presented in [4]. Fig. 4 shows the geometry of the ring on block problem in its initial configuration as well as in its deformed configuration corresponding to the last load step. The problem involves an elastic half-ring divided into two layers of different elastic properties and a rectangular block. Denoting the unit length with UL, the half-ring inner diameter is equal to 90 UL, the thickness of each ring layer is equal to 5 UL, while the block length and height

---

are equal to 260 UL and 50 UL respectively. The initial gap between the ring and the block corresponds to 20 UL. The coarsest mesh utilized in the calculations consists of 64 elements along the ring circumference and 1 element across each ring layer thickness as well as 52 by 10 elements for the block length and height directions respectively.
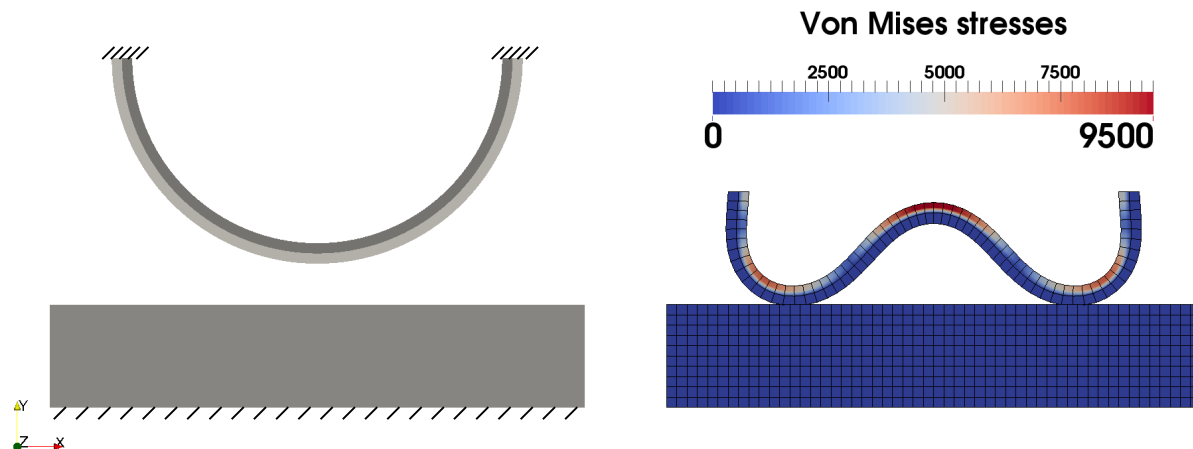

Figure 4: *Initial and deformed configuration for the elastic ring on block problem.*

A homogeneous Dirichlet condition is imposed on the bottom edge of the block, while the loading of the system is introduced through a non-homogeneous Dirichlet condition at the half-ring ends. In total, the vertical displacement of the half-ring ends is varied from -20 UL to -65 UL in steps of 0.5 UL, while the corresponding horizontal displacement is kept zero. As in reference [15], neo-Hookean behavior is assumed for both the ring and the block materials. Referring to the unit force with UF, the Young's moduli for the inner and outer half-ring layers are equal to 10^5 and 10^3 UF/UL^2 respectively and equal to 10^8 UF/UL^2 for the block. Poisson's ratio is assumed equal to 0.3 for both ring layers and equal to zero for the block. The contact between the ring and the block is assumed to be frictionless.

The deformed configuration shown in Fig. 4 was calculated with a quadratic finite element approximation of the geometry and the displacement field and a linear approximation for the Lagrange multiplier corresponding to the contact stress. The external ring edge was defined as the slave surface and the top block edge was defined as the master surface. An augmentation parameter equal to 1000 was utilized. Fig. 5 shows the evolution of the vertical displacement of the half-ring middle point during the last 50 load steps, calculated for three different values of the augmentation parameter, 10^2, 10^3 and 10^5. The required Newton iterations per load step are presented for the whole simulation in Fig. 6.

The conducted variation of the augmentation parameter has no significant impact on the observed deformation of the ring. Approximately until the 50th load step, the half-ring middle point remains in contact with the block surface. Beyond that point, the half-ring starts to fold and its middle is lifted from the block surface progressively until approximately the 75th load step. The process is accelerated afterwards towards the deformed configuration shown in Fig. 4 with the middle point lifting velocity reaching its maximum around the 80th load step. At the same point the sliding velocity in the contact between the ring and the block becomes maximum as well.

Within the studied range, the augmentation parameter value did not affect convergence of the iterative solution. In large portion of the simulation, four Newton iterations are sufficient for decreasing the relative residual norm below the level of 10^{-8}. Close to the 80th load step, an increased number of Newton iterations are required, but without exceeding the number of 8 iterations in any case.
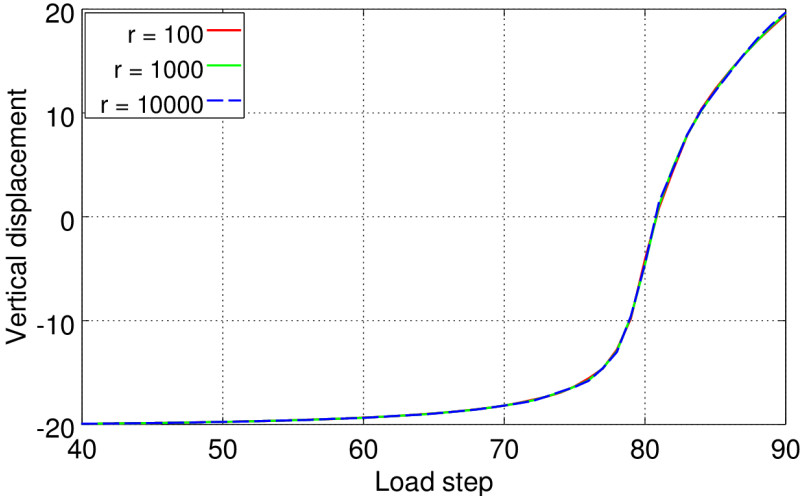

Figure 5: *Vertical displacement of the half-ring middle point for different augmentation parameter values and a quadratic geometrical approximation, during the last 50 load steps.*
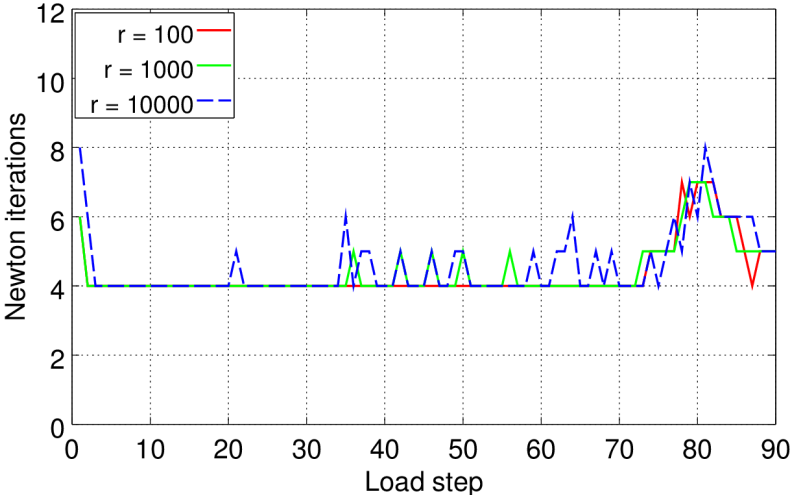

Figure 6: *Number of required Newton iterations per load step for different augmentation parameter values and a quadratic geometrical approximation.*

A calculation with a mesh refined by a factor of two, yields results similar to the original simulation. For the default augmentation parameter value of 1000, Fig. 7 compares the convergence behavior between the original and the refined mesh. Comparable convergence behaviors
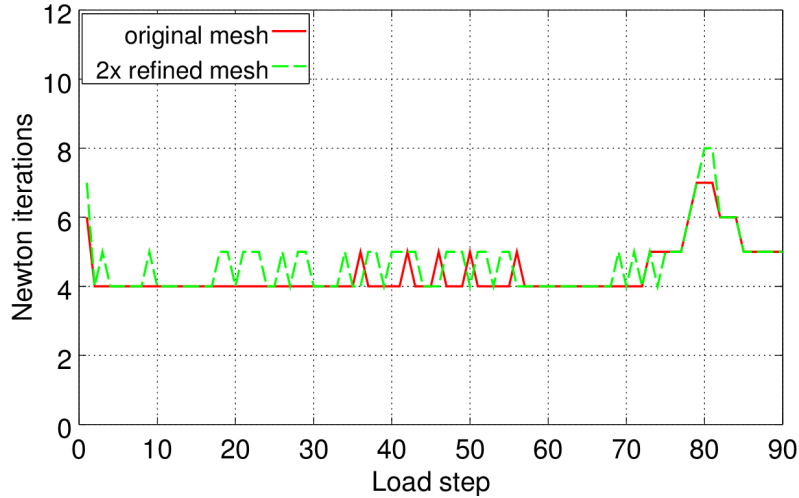
were observed with both mesh sizes.

Figure 7: *Number of required Newton iterations per load step for different mesh sizes and a quadratic geometrical approximation.*

All results presented with respect to the first numerical example are based on numerical integration with three Gauss points per mesh edge. It has been observed however, that reducing the number of Gauss points to two or increasing it to four, has little impact on the numerical results. Furthermore, defining the slave surface on the block instead of the ring side yields similar results.

8.2 Shallow ironing

The second numerical example to be presented is the so called shallow ironing problem. It consists of an indenter with an arc shaped bottom edge pressed against a rectangular slab and being slid along the slab length. Also this example is presented in [15] and [4]. Fig. 8 shows the initial and deformed geometry at different phases of the solution. Materials exhibit, like in the first example, neo-Hookean behavior with Young's moduli equal to $68.96 \cdot 10^8$ and $68.96 \cdot 10^7$ UF/UL^2 for the indenter and the slab respectively and Poisson's ratio for both parts equal to 0.32. The coefficient of friction between the two parts is equal to 0.3.

The contact between the indenter and the slab is solved as a quasi-static problem. Nevertheless, for the sake of presentation of the results, load steps are defined as a function of time. From 0 to 1 time units T, the indenter is moved vertically towards the slab by a total amount of 1 UL in 10 equal steps. From time 1 T until time 2 T, the indenter is displaced horizontally by a total distance of 10 UL in 500 equal steps.

Fig. 9 shows the evolution of the total horizontal and vertical force components between the contacting bodies, during the simulated period. Apart from the default case with friction, results for the frictionless case are also included for comparison. The results presented in both Fig. 8 and Fig. 9 are based on a quadratic finite element approximation of the geometry and the displacements field and a linear approximation of the contact stress. Three Gauss points per segment are used for numerical integration and the indenter surface is defined as the slave surface.
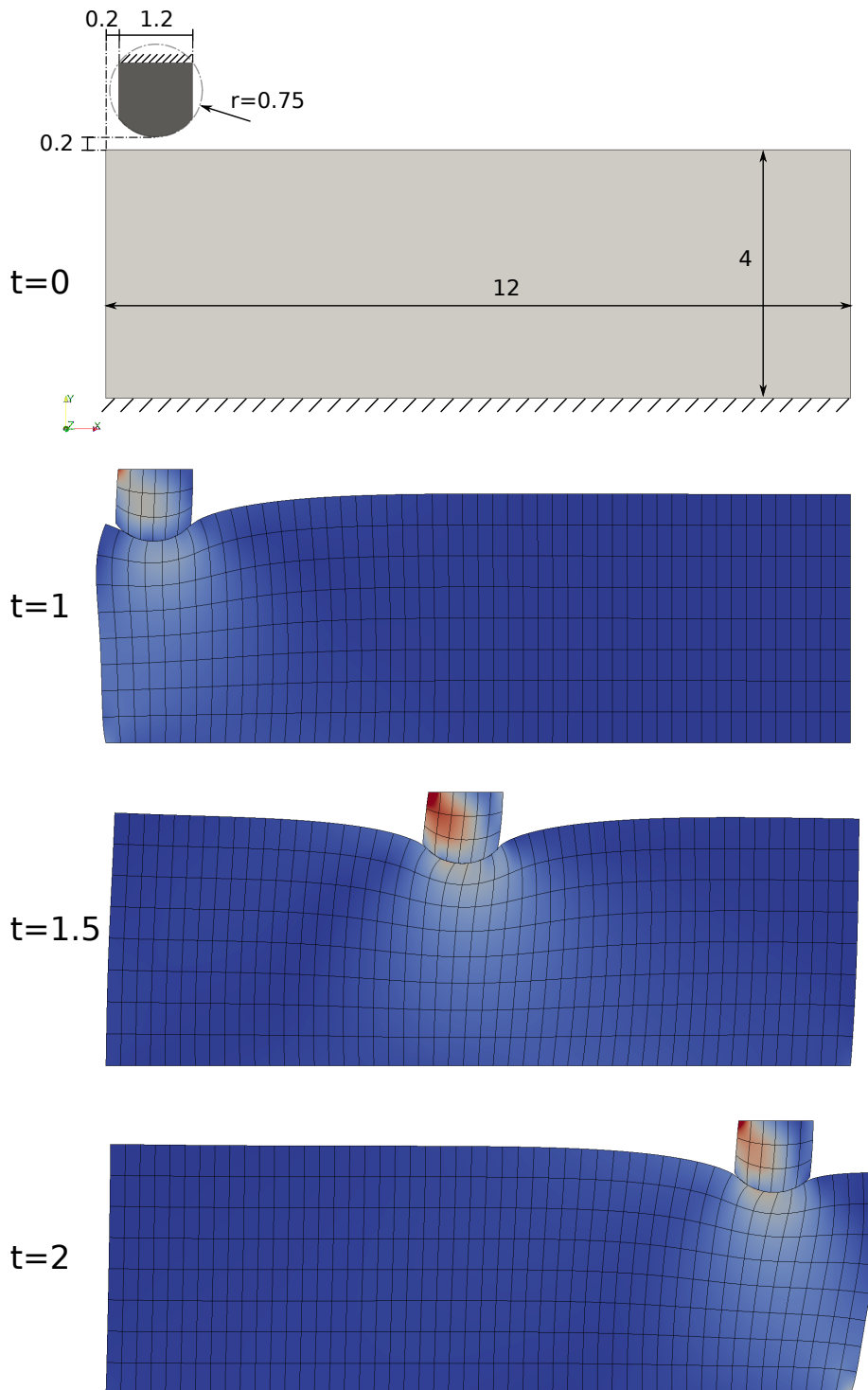
Figure 8: *Initial and deformed configurations for the shallow ironing problem.*
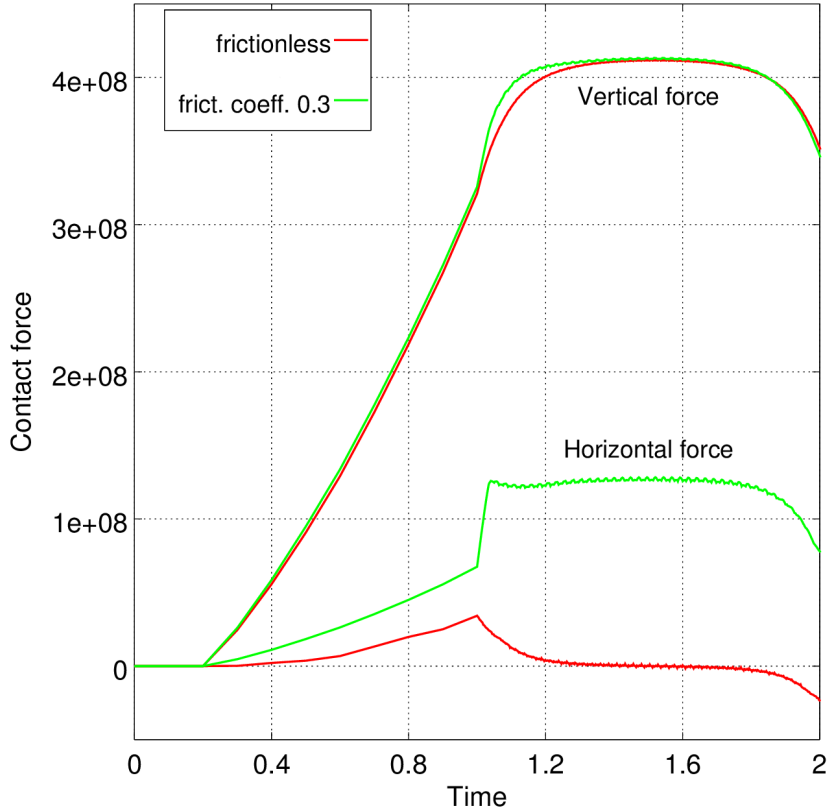
Figure 9: *Calculated vertical and horizontal contact forces for the shallow ironing example with and without friction.*

In comparison with previously published results, the vertical force in Fig. 9 is slightly higher than in [4] and significantly higher than in [15], while the reported horizontal force is significantly lower than in both aforementioned references. Nevertheless, the form of the curves in Fig. 9 is similar to the corresponding ones found in [15] and [4].

For a better comparison, the ratio between the horizontal and vertical force at time 1.5 T can be considered. A ratio of 0.53 can be estimated from the results reported in [15], a ratio of 0.39 according to reference [4], while Fig. 9 corresponds to a ratio of only 0.31. In order to provide the possibility of investigating the source of the observed discrepancies, Fig. 10 illustrates the calculated contact stresses field at time 1.5 T. The contact stress distribution is according to common understanding of the system mechanics and the angle between the stress vectors and the surface normals appears to be very close to the friction angle of $16.7°$ corresponding to the given coefficient of friction of 0.3. Moreover, for the frictionless case reported in Fig. 9, a zero horizontal force is predicted for the symmetric position at 1.5 T, correctly.
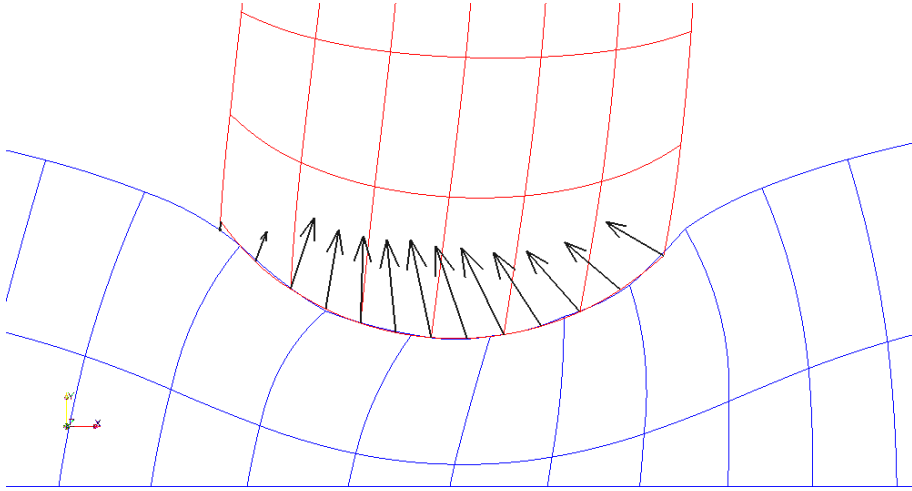
Figure 10: *Calculated deformations and contact stresses at time 1.5 T.*

Results similar to those presented in Fig. 9 could be produced with finer mesh size, different finite element approximations and different numbers of Gauss points. In all cases the number of Newton iterations per load step remains approximately constant in the period from 1 T until 2 T. Tables 1 and 2 summarize the average number of Newton iterations per load step for different cases without and with friction respectively. The first row of each table corresponds to one of the cases presented in Fig. 9 while each further row contains the parameters that differentiate every individual case from the first row.

Table 1: Average number of Newton iterations from 1 to 2 T for different cases (frictionless).

Mesh size	Displacements FEM order	Contact stress FEM order	Gauss points	Augmentation parameter	Newton iterations
1x	**2**	**1**	**3**	$\mathbf{10^3}$	**4.7**
	1				4.3
		2			5.0
2x	1				4.9
2x					5.0
	1		2		4.4
			2		4.9
	1		4		4.3
			4		4.5
				10^2	4.6
				10^4	4.7

16

Table 2: Average number of Newton iterations from 1 to 2 T for different cases (friction coefficient of 0.3).

Mesh size	Displacements FEM order	Contact stress FEM order	Gauss points	Augmentation parameter	Newton iterations
1x	**2**	**1**	**3**	**10^3**	**5.9**
	1				4.7
		2			6.6
2x	1				5.5
2x					6.0
	1		2		4.5
			2		6.0
	1		4		4.6
			4		5.4
				10^2	5.9
				10^4	5.1

In general, all reported cases deliver comparable convergence performance. The averagely required Newton iterations per load step vary in the frictionless cases from 4.3 to 5, while in the cases with friction, 4.7 to 6.6 iterations are required. However, the accuracy of the result may depend significantly on the specific choice of solution parameters. As an example, Fig. 11 compares the contact forces calculated with 2 and 4 Gauss points per segment, for the case with friction and quadratic approximation of displacements. In comparison to the equivalent result presented in Fig. 9, which is based on 3 Gauss points, the calculation with 4 Gauss points provides a completely free of oscillations solution, while the solution with only 2 Gauss points per segment exhibits more pronounced oscillations of the calculated force, with wavelength equal to the mesh size. Nevertheless, the observed oscillations even with only 2 Gauss points are still relatively small, compared to similar results presented in [15] and [4].
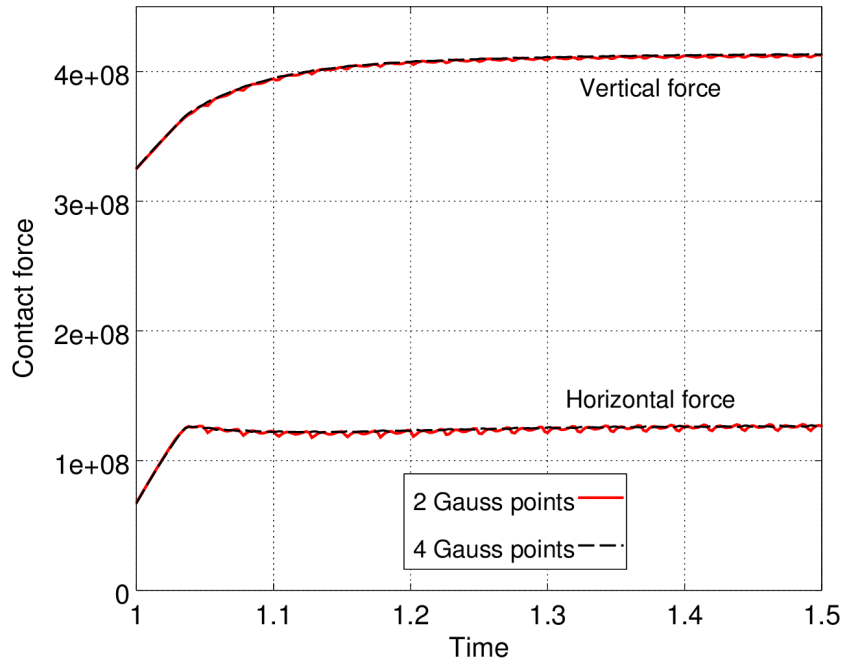
Figure 11: *Calculated vertical and horizontal contact forces for the shallow ironing example and different numbers of Gauss points.*

8.3 Crossed tubes

The last numerical example refers to the contact between two crossed hollow cylinders. Each of these tubes has an outer diameter of 12 UL, wall thickness equal to 0.8 UL and length equal to 100 UL. Neo-Hookean material behavior is assumed for both tubes, with material parameters corresponding to Poisson's ratio equal to 0.3 as well as Young's moduli of 10^5 UF/UL^2 for the lower tube and 10^4 UF/UL^2 for the upper one.

The lower tube oriented with its axis parallel to the z direction and the upper tube with its axis parallel to the x direction are forced into contact through Dirichlet conditions applied on their free ends. Relatively to their initial configuration shown in Fig. 12, the ends of the lower tube remain fixed while the upper tube is moved vertically. In a preliminary step, the upper tube is lowered by 20 UL, corresponding to the initial gap between the tubes while in 80 further equal size steps, the ends of the upper tube are lowered by another 40 UL.
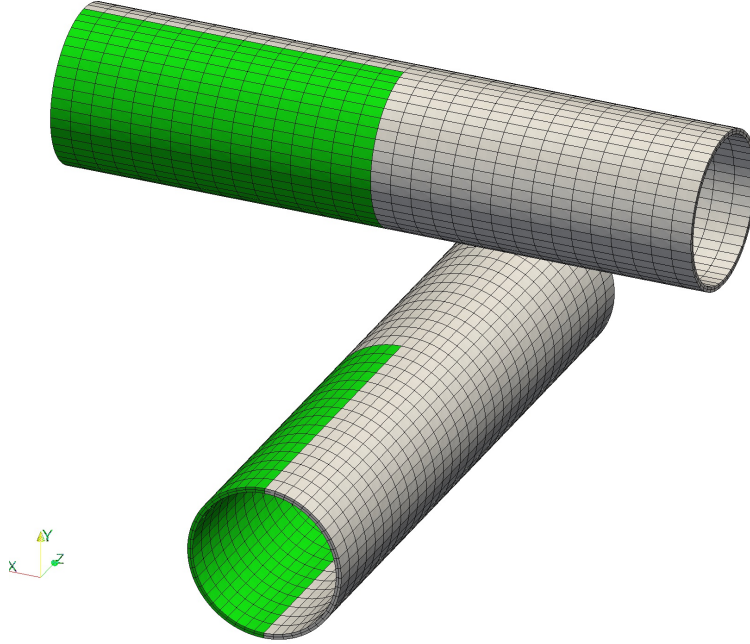
Figure 12: *Geometry and mesh of the crossed tubes in their initial configuration.*

Due to symmetric geometry and boundary conditions it is sufficient to model only one quarter of the considered structure. The actually modeled portion of each tube is identified in Fig. 12 colored in green and is discretized with 16 by 24 by 2 elements in the length, circumferential and radial directions respectively. Fig. 13 shows the calculated deformed configurations for the 40th, 60th and 80th load steps. The presented solution is based on an approximation of the geometry and the displacement field with incomplete second order 20-node hexahedral elements. For the contact condition between the two tubes, the outer surface of the lower tube is considered as the slave surface. For the self-contact condition in the interior of the upper tube, its internal surface is considered as both slave and master surface at the same time. The contact stresses are approximated through linear elements on each of the slave surfaces, corresponding to faces of 8-node hexahedral elements. Numerical integration of contact terms is carried out based on nine Gauss points per element face.

The results presented in Fig. 13 correspond to frictionless contact conditions while Fig. 14, shows the required Newton iterations for the frictionless case as well as for a friction coefficient of 0.15. Despite the lack of stabilization for dealing with a possible violation of the inf-sup condition related to the self-contact in the interior of the upper tube, the Newton algorithm converges in general fast. Only exception is the 61st load step, which actually corresponds to the onset of self contact in the interior of the upper tube. It is expected that applying an appropriate stabilization technique will help in achieving a good convergence at this single point as well.
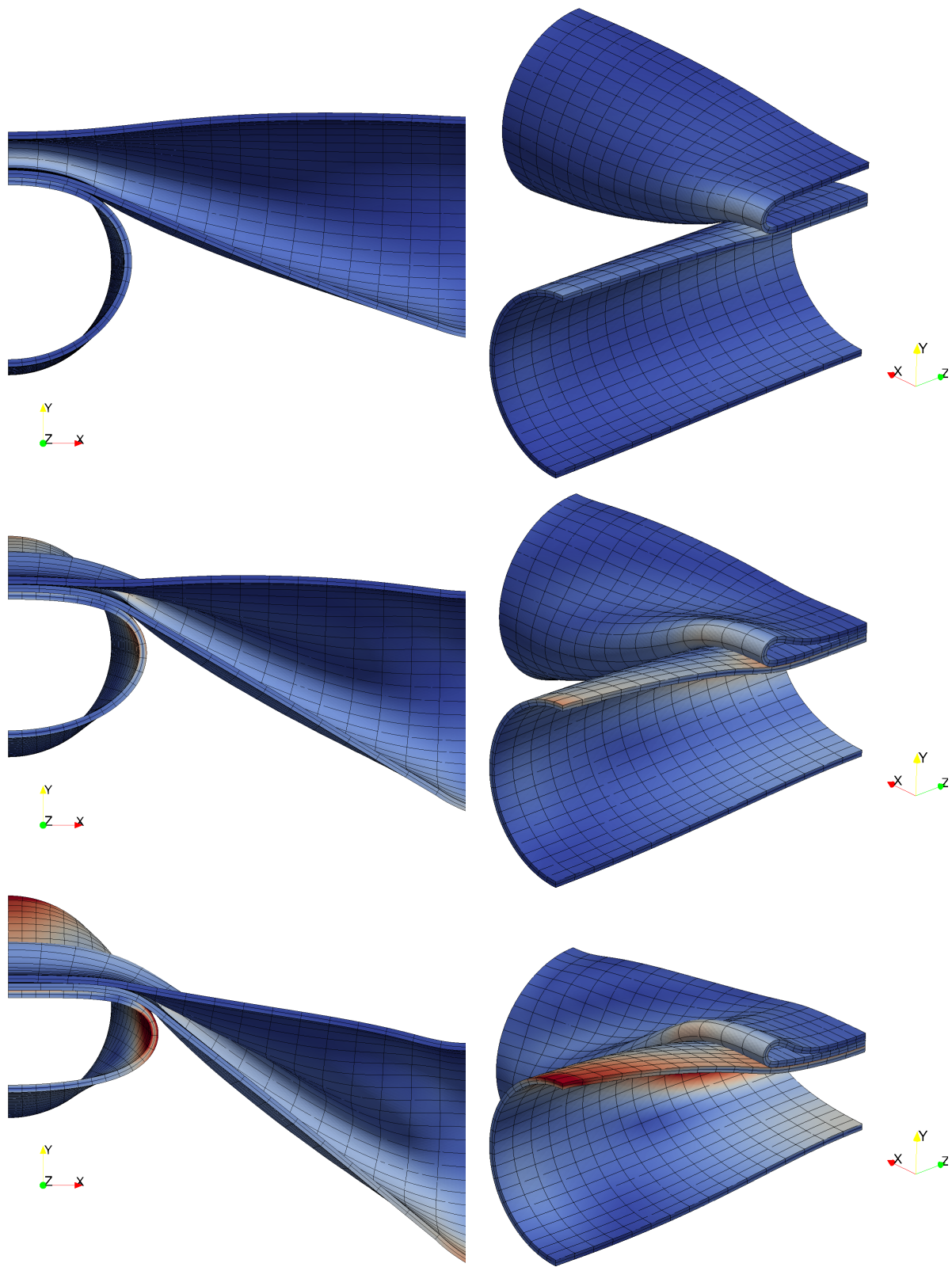
Figure 13: *Deformed configuration of the crossed tubes in contact at 20, 30 and 40 UL of relative displacement between the tubes (top, middle and bottom respectively).*
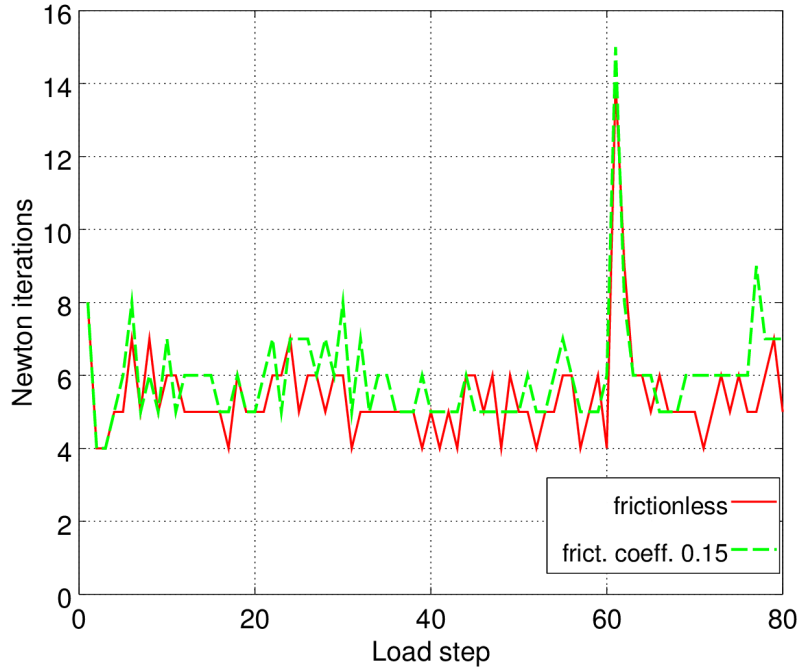
20

Figure 14: *Number of required Newton iterations per load step without and with friction.*

9 Concluding remarks

In this paper we presented a new approximation of the frictional contact condition between deformable bodies under finite deformations and large sliding. The main characteristics of the proposed formulation are: 1) the relative simplicity of the tangent system, 2) the independence on the utilized finite element method and 3) its locking-free behavior. The simplicity of the formulation consists in the facts that the tangent system does not depend on the curvature of the contact surfaces, no special treatment of corners and edges is required and the contact condition is expressed in Cartesian coordinates. As a consequence of the independence on the finite element method, the formulation could be used with complex methods such as iso-geometrical or enriched elements without any additional treatment. A price for the simplicity of the tangent system is its non-symmetry.

The term "ray-tracing" was used in this paper to describe the inverse projection that the proposed formulation is based on. We suggest this term as an identifier for contact formulations that define the contact normals and the Lagrange multipliers on the same surface (slave). Identifying such contact formulations as a distinct category is important for studying them in the future more systematically in order to evaluate their potential advantages and disadvantages in general.

A series of two and three-dimensional examples were presented in order to demonstrate the robustness of the proposed formulation. Numerical integration with a relatively low number of Gauss points per contact face was sufficient for delivering satisfactory results in terms of accuracy and convergence. Regarding the applicability of the formulation in cases of self-contact, the corresponding numerical example indicated poor convergence only during the onset of self-contact. In order to improve this limitation, the contact formulation should be extended in the

future through an appropriate stabilization technique in order to deal with a possible violation of the inf-sup condition between the contact stress and displacement approximations.

Appendix A: Partial derivatives of the map $F(\lambda, g, V^r, n)$

Let $\tau = \mathscr{F}(\lambda \cdot n + rg)_-$ and $H(x)$ the Heaviside function ($H(x) = 1$ for $x \geq 0$ and $H(x) = 0$ for $x < 0$), then

$$
\begin{aligned}
\delta_\lambda F(\lambda, g, V^r, n_x) &= \delta_v P_{B_T(\tau)} + \delta_\tau P_{B_T(\tau)} \otimes \delta_\lambda \tau + H(-\lambda \cdot n - rg) n \otimes n, \\
\delta_g F(\lambda, g, V^r, n_x) &= \delta_\tau P_{B_T(\tau)} \delta_g \tau + H(-\lambda \cdot n - rg) rn, \\
\delta_n F(\lambda, g, V^r, n_x) &= \delta_n P_{B_T(\tau)} + \delta_\tau P_{B_T(\tau)} \otimes \delta_n \tau \\
&\quad + H(-\lambda \cdot n - rg) \left(n \otimes \lambda - (2\lambda \cdot n + rg) n \otimes n + (\lambda \cdot n + rg) I \right), \\
\delta_{V^r} F(\lambda, g, V^r, n_x) &= -r \delta_v P_{B_T(\tau)},
\end{aligned}
$$

and, denoting $v_T = (I - n \otimes n) v$ for simplicity,

$$
\delta_v P_{B_T(\tau)}(v) = \left|
\begin{array}{l}
0 \text{ when } \tau \leq 0, \\
I - n \otimes n \text{ when } \|v_T\| \leq \tau, \\
\dfrac{\tau}{\|v_T\|} \left(I - \dfrac{v_T}{\|v_T\|} \otimes \dfrac{v_T}{\|v_T\|} - n \otimes n \right) \text{ otherwise,}
\end{array}
\right.
$$

$$
\delta_\tau P_{B_T(\tau)}(v) = \left|
\begin{array}{l}
0 \text{ when } \tau \leq 0 \text{ or } \|v_T\| \leq \tau, \\
\dfrac{v_T}{\|v_T\|} \text{ otherwise,}
\end{array}
\right.
$$

$$
\delta_n P_{B_T(\tau)}(v) = \left|
\begin{array}{l}
0 \text{ when } \tau \leq 0, \\
-v \cdot n (I - n \otimes n) - n \otimes v_T \text{ when } \|v_T\| \leq \tau, \\
-\dfrac{\tau}{\|v_T\|} \left(v \cdot n \left(I - \dfrac{v_T}{\|v_T\|} \otimes \dfrac{v_T}{\|v_T\|} - n \otimes n \right) + n \otimes v_T \right) \text{ otherwise,}
\end{array}
\right.
$$

$$
\begin{aligned}
\delta_\lambda \tau &= -H(-\lambda \cdot n - rg) \mathscr{F} n, \\
\delta_g \tau &= -H(-\lambda \cdot n - rg) \mathscr{F} r, \\
\delta_n \tau &= -H(-\lambda \cdot n - rg) \mathscr{F} (I - n \otimes n) \lambda.
\end{aligned}
$$

References

[1] P. Alart, A. Curnier. A generalized Newton method for contact problems with friction. *J. Mech. Theor. Appl.*, 7:1 (1988), 67–82.

[2] T. Dickopf, R. Krause. Efficient simulation of multi-body contact problems on complex geometries: a flexible decomposition approach using constrained minimization. *Int. J. Numer. Meth. Engng.* 77 (2009), 1834–1862.

[3] G. Haikal, K.D. Hjelmstad. A finite element formulation of non-smooth contact based on oriented volumes for quadrilateral and hexahedral elements. *Comput. Methods Appl. Mech. Engrg.* 196 (2007), 4690–4711.

[4] S. Hartmann, J. Oliver, R. Weyler, J.C. Cante, J.A. Hernández. A contact domain method for large deformation frictional contact problems. Part 2: Numerical aspects. *Comput. Methods Appl. Mech. Engrg.* 198 (2009), 2607–2631.

[5] E. Hermann, F. Faure, B. Raffin. Ray-traced collision detection for deformable bodies. *3rd International Conference on Computer Graphics Theory and Applications (GRAPP)*, Madeira, 2008.

[6] A. Konyukhov, K. Schweizerhof. *Computational Contact Mechanics.* Lecture Notes in Applied and Computational Mechanics, vol. 67, Springer-Verlag, Berlin 2013.

[7] P. Laborde, Y. Renard. Fixed point strategies for elastostatic frictional contact problems. *Math. Meth. Appl. Sci.*, 31 (2008), 415–441.

[8] T.A. Laursen. *Computational Contact and Impact Mechanics.* Springer-Verlag, Berlin 2003.

[9] J.T. Oden, S.J. Kim. Interior penaty methods for finite element approximations of the Signorini problem in elastostatics. *Comp. and Maths. with Appls.*, 8:1 (1982), 35–56.

[10] J. Oliver, S. Hartmann, J.C. Cante, R. Weyler, J.A. Hernández. A contact domain method for large deformation frictional contact problems. Part 1: Theoretical basis. *Comput. Methods Appl. Mech. Engrg.* 198 (2009), 2591–2606.

[11] M.A. Puso, T.A. Laursen. A mortar segment-to-segment contact method for large deformation solid mechanics. *Comput. Methods Appl. Mech. Engrg.* 193 (2004), 601–629.

[12] Y. Renard. Generalized Newton's methods for the approximation and resolution of frictional contact problems in elasticity. *Comput. Methods Appl. Mech. Engrg.*, 256 (2013), 38–55.

[13] M. Siavelis, P. Massin, M.L.E. Guiton, S. Mazet, N. Moes. Robust implementation of contact under friction and large sliding with the extended nite element method. *Eur. J. Comp. Mech.*, 19:1-2-3(2010), 189–203.

[14] S.P. Wang, E. Nakamachi. The inside-outside contact search algorithm for finite element analysis. *Int. J. Numer. Meth. Engng.*, 40 (1997), 3665–3685.

[15] P. Wriggers. *Computational Contact Mechanics, Second Edition.* Springer-Verlag, Berlin 2006.

[16] P. Wriggers, J. Schroeder, A. Schwarz. A finite element method for contact using a third medium. *Comput. Mech.*, 52:4(2013), 837–847.

[17] B. Yang, T.A. Laursen, X. Meng. Two dimensional mortar contact methods for large deformation frictional sliding. *Int. J. Numer. Meth. Engng.*, 62 (2005), 1182–1225.

[18] G. Zavarise, P. Wriggers. A Segment-to-Segment Contact Strategy. *Mathl. Comput. Modelling*, 28:4–8 (1998), 497–515.